Elliptical optical solitary waves in a finite nematic liquid crystal cell

Elliptical optical solitary waves in a finite nematic liquid crystal cell

Antonmaria A. Minzoni[a], Luke W. Sciberras[b,a,*], Noel F. Smyth[c], Annette L. Worthy[b]

[a] *Fenomenos Nonlineales y Mecánica (FENOMEC), Department of Mathematics and Mechanics, Instituto de Investigacion en Matemáticas Aplicadas y Sistemas, Universidad Nacional Autónoma de México, 01000 México D.F., México*

[b] *School of Mathematics and Applied Statistics, University of Wollongong, Northfields Avenue, Wollongong, New South Wales, Australia, 2522.*

[c] *School of Mathematics and Maxwell Institute for Mathematical Sciences, University of Edinburgh, Edinburgh EH9 3JZ, Scotland, U.K.*

Abstract

The addition of orbital angular momentum has been previously shown to stabilise beams of elliptic cross-section. In this article the evolution of such elliptical beams is explored through the use of an approximate methodology based on modulation theory. An approximate method is used as the equations that govern the optical system have no known exact solitary wave solution. This study brings to light two distinct phases in the evolution of a beam carrying orbital angular momentum. The two phases are determined by the shedding of radiation in the form of mass loss and angular momentum loss. The first phase is dominated by the shedding of angular momentum loss through spiral waves. The second phase is dominated by diffractive radiation loss which drives the elliptical solitary wave to a steady state. In addition to modulation theory, the "chirp" variational method is also used to study this evolution. Due to the significant role radiation loss plays in the evolution of an elliptical solitary wave, an attempt is made to couple radiation loss to the chirp variational method. This attempt furthers understanding as to why radiation loss cannot be coupled to the chirp method. The basic reason for this is that there is no consistent manner to match the chirp trial function to the generated radiating waves which is uniformly valid in time. Finally, full numerical solutions of the governing equations are compared with solutions obtained using the various variational approximations, with the best agreement achieved with modulation theory due to its ability to include both mass and angular momentum loss to shed diffractive radiation.

Keywords: Liquid crystal, soliton, elliptic solitary wave, nematicon, modulation theory

1. Introduction

The propagation of a bulk optical solitary wave in a nematic liquid crystal, a so-called nematicon [1], has become an active area of study [2, 3] since their first experimental

*Corresponding author

Email address: lws31@uowmail.edu.au (Luke W. Sciberras)

demonstration [4]. These studies are more general, however, as the equations governing bulk optical solitary waves in a nematic liquid crystal also apply to bulk solitary waves in thermal media [5], photorefractive crystals and other optically active bulk media [6]. A similar system of equations to that governing these bulk optical solitary waves arises in α models of fluid turbulence [7, 8]. Nearly all of these optical studies have dealt with circularly symmetric beams, however. Elliptical bulk optical solitary waves introduce new mechanisms and effects not encountered with circularly symmetric beams.

The propagation of an elliptical cross-section beam in local media has been an experimental [9, 10] and theoretical issue [11–13]. In local media, such beams are described by nonlinear Schrödinger (NLS)-type equations [11–13]. In addition to the standard instability of two dimensional solitary waves governed by nonlinear Schrödinger equations [6, 14], there is an additional instability of elliptical beams due to the existence of the different major and minor axes of such optical beams, as the amount of nonlinearity required to support a radially symmetric solitary wave is dependent on the peak beam intensity [10]. Hence, the peak beam intensity also determines the diffraction angle that must balance with the self-focusing of the optical beam to self-trap [1, 2] and thus form a solitary wave. For an optical beam to self-trap, radial symmetry is then required. However, an elliptical beam is asymmetric and, hence, difficulties arise in the support required for the two competing diffraction angles [10, 11]. The term elliptic solitary wave will be used from here on to describe an elliptical cross-section solitary wave. Further, adding to the difficulty in forming an elliptic solitary wave, it has been shown both experimentally [9, 10, 15] and theoretically [11–13] that the widths of the elliptic beam periodically oscillate, as would be expected from the general behaviour of beams for NLS-type equations.

Several methods have been suggested to aid in the formation and stabilisation of an elliptic solitary wave before it diffracts into a circularly symmetric beam. Examples are to use partially incoherent elliptic beams with an anisotropic mutual coherence function [9, 10], a medium with a nonlocal response [12, 16] or applying an orbital angular momentum to the elliptic-shaped beam [13]. The propagation of an elliptic solitary wave in the nonlocal medium of a nematic liquid crystal (NLC) [2] is the subject of this work.

Elliptic solitons have been shown to exist in a nematic liquid crystal [16], which is an example of a nonlocal, nonlinear medium [2]. The key to the behaviour of an elliptic solitary wave in a nematic liquid crystal is the self-focusing response of an NLC. A nematic molecule tends to align itself with the direction of an electric field, whether this is an external bias field applied across the liquid crystal cell or that of an optical beam input into the cell [2, 17]. If the optical beam is of sufficient power to overcome the Freédericksz threshold [2, 17–19] the nematic molecules will rotate, thus altering the refractive index of the NLC. If the refractive index increases, this self-focusing response of the beam can balance diffraction, resulting in a solitary wave, or nematicon [2, 3]. In addition, it has been shown that nematic molecules tend to align with the major axis of an elliptic beam [16]. However, the issue of the stability of elliptic beams has not been addressed.

In the present work, an elliptical cross-section optical beam with orbital angular momentum propagating through a finite sized nonlocal NLC cell is studied. As stated above, to induce the self-focusing response of the NLC, the optical beam intensity must be above the minimum to enable the nematic molecules to rotate, the Freédericksz threshold [2, 17–19]. To enable the use of milliwatt beam powers a pre-tilt is induced within the

NLC so the molecules form an angle $\theta_0 \sim \pi/4$ with the optical wavefront, with the Freédericksz threshold reduced to exactly zero when $\pi/4$. In this manner, milliwatt optical beam powers induce a sufficient change in the nematic's refractive index [20] to enable a nematicon to form. There are two main techniques for applying the desired pre-tilt angle. The first is to apply an external static electric field perpendicular to the optical axis in the direction of polarisation of the optical field. The second technique creates a static charge on the cell walls by "rubbing" them, thus causing the nematic molecules near the cell walls to rotate [2]. This tilt angle is then transferred throughout the bulk of the NLC cell by the intermolecular elastic links [2]. Rubbing the cell walls to pre-tilt the nematic molecules results in different decay rates of the nematic response to the optical beam. In one transverse dimension a linear decay is experienced [21], while in two transverse dimensions [22, 23] a logarithmic decay results. This implies that the nematic response to the beam extends to the boundaries of the NLC cell and, as a result, the inclusion of proper boundary conditions is vital in order to model an elliptic solitary wave accurately.

The present work will focus on the role diffractive radiation and orbital angular momentum shed to diffractive radiation play in the evolution of an elliptical nematicon. While it has been found that angular momentum can stabilise an elliptical nematicon for short evolution distances [13], typically $\sim$ 5–10 revolutions of the major axis, it has been found that on longer scales, which amount to $\sim$ 100 rotations, that angular momentum loss to diffractive radiation causes the elliptical solitary wave to become circular and stop rotating. In addition to this effect of shed diffractive radiation, the effect the boundaries have on the evolution of elliptic solitary waves will also be investigated. This analysis will be based on using an exact solution for the director distribution and modulation equations [24] for the optical field derived using suitable trial functions [25, 26] in a Lagrangian representation of the governing equations. Modulation theory has proved to be a successful technique for modelling the evolution of nonlinear optical beams in NLC, giving excellent agreement with full numerical solutions of the governing equations [27–33] and with experimental results [34–36]. In the present work we show how the shed diffractive radiation can be studied using geometric optics. We obtain approximate evolution equations for the elliptical solitary wave parameters which explain the relevant features of the processes observed in numerical solutions.

2. Governing Equations

Consider a polarised, coherent elliptical cross-sectional optical beam input into a finite sized NLC cell. Let us take the z direction as the propagation direction. The nematic molecules are arranged in a planar configuration within the NLC cell. The optical beam is polarised in the x direction, which results in molecular rotation in the (x, z) plane [1, 2, 4, 37, 38]. The nematic molecules are pre-tilted by a angle $\theta_0 \sim \pi/4$ in the (x, z) plane [20], enabling the use of milliwatt beam powers, as the Freédericksz threshold is thus overcome [2, 17–19]. The pre-tilt of the nematic is achieved by rubbing the cell walls. The intermolecular elastic forces of the NLC pass the rotation then achieved through the bulk of the medium, thus obtaining a semi-uniform pre-tilt. The optical beam's electric field causes a further rotation of the director by an angle θ, so that the total director angle is given by $\phi = \theta_0 + \theta$, relative to the z axis. The perturbation of the director due to the optical beam is small for milliwatt beam powers, $|\theta| \ll |\theta_0|$. The non-dimensional

equations governing the propagation of the optical beam in this small extra rotation limit in the paraxial approximation are a strongly coupled pair of partial differential equations (PDEs), the first of which is an NLS-like equation for the optical beams and the second is Poisson's equation for the director rotation [21, 22, 39, 40], these being

$$iE_z + \frac{1}{2}\nabla^2 E + 2\theta E = 0, \tag{1}$$

$$\nu\nabla^2\theta + 2|E|^2 = 0. \tag{2}$$

The Laplacian ∇^2 is in the (x, y) plane and E is the complex valued envelope of the electric field. The elastic response of the NLC is given by the nonlocality parameter ν, which is experimentally $O(100)$ [34]. In experiments, the optical beam experiences a phenomenon known as walk-off due to the refractive index being a tensor [24], whereby the optical beam deviates from the input wavevector along the z direction and follows the beam's Poynting vector. This walk-off has been removed from the the electric field equation (1) by using a phase transformation of the electric field [27]. The NLC cell is finite sized and is a rectangle with dimensions $0 \leq x \leq L_x$ and $0 \leq y \leq L_y$.

The governing equations (1) and (2) have the Lagrangian representation

$$L = i(E^* E_z - E E_z^*) - |\nabla E|^2 + 4\theta|E|^2 - \nu|\nabla\theta|^2, \tag{3}$$

where the * superscript denotes the complex conjugate. The boundary conditions are taken to be homogeneous for both E and θ.

In the next section two different trial functions will be used to obtain approximate evolution equations for the elliptical solitary wave, based on the Lagrangian (3) [22, 29, 40–42]. In both cases the director equation (2) is solved using Fourier series. The averaged Lagrangian will then provide consistent modulation equations which will be coupled to radiation loss.

3. Trial functions and approximate evolution equations

The governing equations (1) and (2) have no known exact solitary wave solution [3] and, as a result, alternative techniques have been developed to model and study nonlinear optical beam propagation in nematic liquid crystals. One of the more successful of these techniques is modulation theory, which was originally developed for the analysis of slowly varying wavetrains [24]. This technique has been extended to equations which do not have exact nonlinear wave solutions by using suitable trial functions to approximate the wave form in the averaged Lagrangian [26]. As discussed in the Introduction, this technique has been successfully applied to study nonlinear beam propagation in nematic liquid crystals.

In previous studies, a suitable trial function for the envelope of the optical beam's electric field is the Gaussian profile [3, 22, 23]

$$E = ae^{-(x-\xi)^2/w_x^2 - (y-\eta)^2/w_y^2} e^{i\sigma}, \tag{4}$$

where a is the amplitude, w_x is the major axis length, w_y is the minor axis length of the ellipse, (ξ, η) is the centre position within the NLC cell and σ is the phase. All

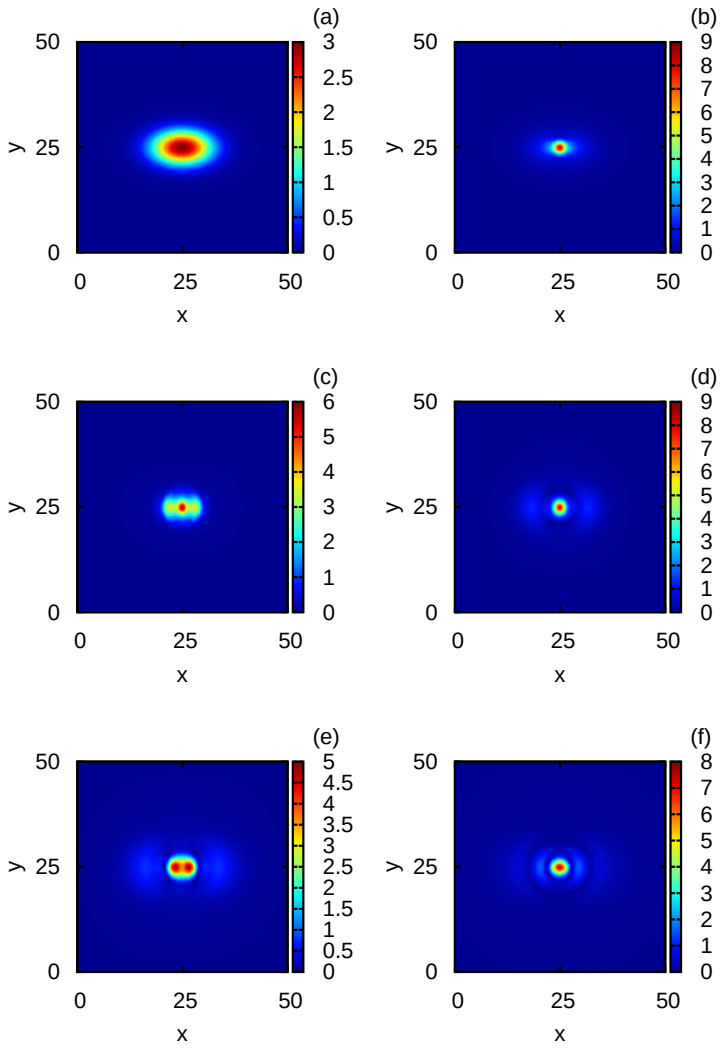

Figure 1: (Colour online) Evolution of an unstable elliptic soliton with no initial tilt and no orbital angular momentum for the nondimensional propagation distances (a) $z = 0$, (b) $z = 5$, (c) $z = 10$, (d) $z = 15$, (e) $z = 20$ and (f) $z = 25$. The dynamics of the elliptic soliton change very rapidly over a short propagation distance with the development of two peaks observed in (e). The initial parameter values are $a = 3$, $w_x = 7$, $w_y = 4$, $\phi = 0$, $\Theta = 0$, $(\xi, \eta) = (25, 25)$ and $(V_x, V_y) = (0, 0)$, with $\nu = 200$ and $(L_x, L_y) = (50, 50)$.

the parameters are functions of z, the propagation variable. This trial function can be justified as in the highly nonlocal limit as $\nu \to \infty$, it can be shown that the nematicon has a Gaussian profile [43].

What differentiates this study from most previous studies of nonlinear optical beam propagation in nematic liquid crystals is the addition of an orbital angular momentum (OAM) term in the phase to allow the beam to rotate [13]. This additional phase term was shown to stop, on short propagation scales ($\sim$ 5 rotations), the collapse experienced by elliptic solitons in Kerr media [11, 13] and NLC, as shown in Figures 1 and 2. Figures 1 and 2 show the evolution of two identical input beams with no OAM, where the second beam is initially tilted by an angle of $\pi/4$, as they propagate through a finite sized NLC cell. The figures highlight the immediacy of the induced instability of the elliptical beam in NLC without any OAM, emphasised by the length of propagation from $z = 0$ to $z = 25$ in both cases. It was also found that the size and dimension of the nematic cell had no influence upon the stability of the propagating elliptic soliton without OAM and similar dynamics were observed to those shown in Figures 1 and 2. However, the advantage of including OAM can be clearly seen from Figure 3, which depicts the evolution of an elliptic soliton with OAM. It can be seen that OAM gives the elliptic soliton stability and, when compared with Figures 1 and 2, it can be seen that the stable propagation distance is longer, in this case $z \sim 200$, and the elliptic soliton does not break up into multiple peaks, as seen in Figures 1(e) and 2(e). Beam evolution over longer propagation distances were simulated and in all cases the beams were found to be stable. As the evolution in these cases is similar to that shown in Figure 3, these further examples are not shown here. In order to study the effect of angular momentum, we introduce a rotating system of coordinates centred at the soliton as follows.

Let us denote the angle the major axis of the elliptical beam makes with the x axis by ϕ. Then coordinates (X, Y) centred on the rotating beam and along its axes are

$$\begin{aligned} X &= (x - \xi)\cos\phi + (y - \eta)\sin\phi, \\ Y &= -(x - \xi)\sin\phi + (y - \eta)\cos\phi. \end{aligned} \tag{5}$$

To obtain the approximate evolution equations we use two different variational approximations. The first one is the chirp approximation [25] and the second is the modulation method with radiation loss [41]. We now consider both approximations in detail.

3.1. Chirp Method

The chirp trial function [25, 26] representing an elliptical nematicon with orbital angular momentum propagating through an NLC cell is given, in the rotating coordinate frame (5), by

$$E_c = ae^{-(X^2/w_x^2 + Y^2/w_y^2)}e^{i(\zeta+\zeta_c)}, \tag{6}$$

where $\zeta = \sigma + V_x(x - \xi) + V_y(y - \eta)$ and $\zeta_c = BX^2 + XY\Theta + CY^2$ [13]. Θ gives an asymmetric phase factor related to the OAM of the beam, (V_x, V_y) is the velocity of the centre of the beam and B and C are related to the chirping of the phase.

The solution of the director equation (2), a Poisson equation, for the director angle perturbation can be calculated in the form of an eigenfunction expansion, with $|E|^2$ given

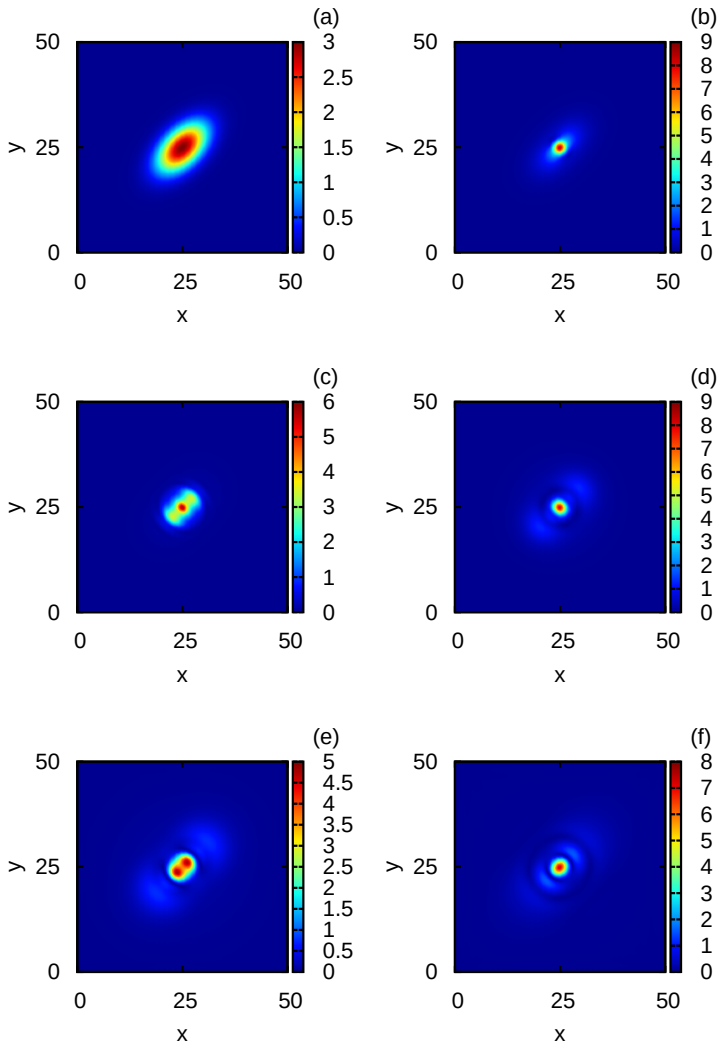

Figure 2: (Colour online) Evolution of an unstable elliptic soliton with an initial tilt of $\pi/4$ and no orbital angular momentum at the nondimensional propagation distances (a) $z = 0$, (b) $z = 5$, (c) $z = 10$, (d) $z = 15$, (e) $z = 20$ and (f) $z = 25$. The dynamics of the elliptic soliton change very rapidly over a short propagation distance with the development of two peaks observed in (e). The initial parameter values are $a = 3$, $w_x = 7$, $w_y = 4$, $\phi = \pi/4$, $\Theta = 0$, $(\xi, \eta) = (25, 25)$ and $(V_x, V_y) = (0, 0)$, with $\nu = 200$ and $(L_x, L_y) = (50, 50)$.

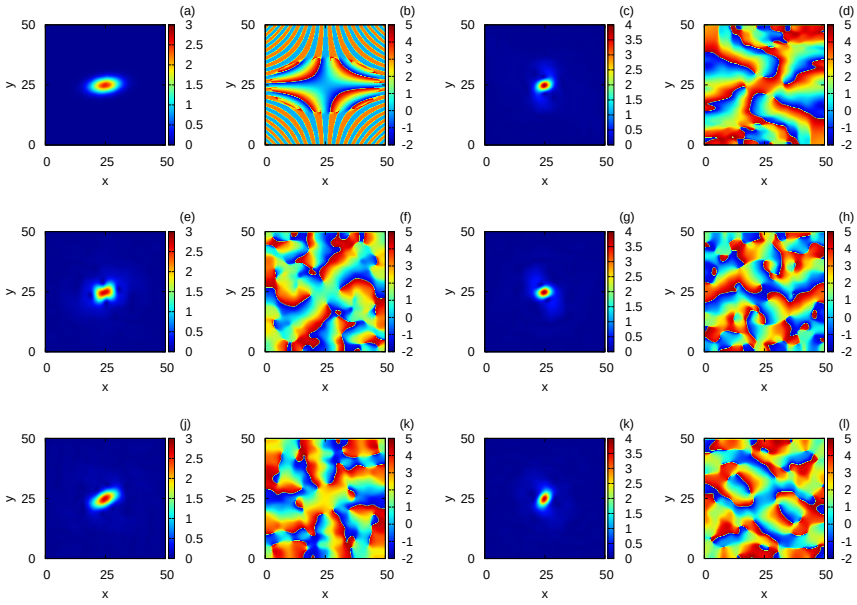

Figure 3: (Colour online) Evolution and phase of an elliptic soliton with no initial tilt for the nondimensional propagation distances (a)–(b) $z = 0$, (c)–(d) $z = 50$, (e)–(f) $z = 100$, (g)–(h) $z = 150$, (i)–(j) $z = 200$ and (k)–(l) $z = 250$. The dynamics of the elliptic soliton are consistent and demonstrate stability induced by the inclusion of OAM. The initial values are $a = 2.5$, $w_x = 6$, $w_y = 3$, $\phi = 0$, $\Theta = 0.07593$, $(\xi, \eta) = (25, 25)$ and $(V_x, V_y) = (0, 0)$, with $\nu = 200$ and $(L_x, L_y) = (50, 50)$.

by (6). This solution is

$$\theta = -\sum_{n,m=1}^{\infty} \frac{C_{nm}}{\pi^2 Q_1} \sin\frac{n\pi x}{L_x} \sin\frac{m\pi y}{L_y}, \tag{7}$$

[22, 23]. The Fourier coefficients of this series are

$$C_{nm} = -\frac{2\pi a^2 w_x w_y}{\nu L_x L_y} \alpha e^{-\gamma_1}, \tag{8}$$

where

$$\gamma_1 = \frac{n^2\pi^2}{8\rho_1 L_x^2}, \quad U_\pm = \frac{\pi^2 w_x^2 w_y^2}{8\rho_1}\psi_\pm^2, \quad \vartheta_\pm = \frac{n\pi\xi}{L_x} \pm \frac{m\pi\eta}{L_y},$$
$$Q_1 = \frac{n^2}{L_x^2} + \frac{m^2}{L_y^2}, \rho_1 = \frac{\cos^2\phi}{w_x^2} + \frac{\sin^2\phi}{w_y^2}, \quad \rho_3 = \cos\phi\sin\phi\left(\frac{1}{w_x^2} - \frac{1}{w_y^2}\right),$$
$$\alpha = \left(e^{-U_+}\cos\vartheta_- - e^{-U_-}\cos\vartheta_+\right) \text{ and } \psi_\pm = \left(\frac{\rho_3 n}{L_x} \pm \frac{\rho_1 m}{L_y}\right).$$

Substituting the trial function (6) for the electric field and the director solution (7) into the Lagrangian (3) and averaging by integrating in x from 0 to L_x and in y from 0 to L_y [24], that is, over the nematic cell, gives the averaged Lagrangian

$$\begin{aligned}\mathcal{L} &= \int_0^{L_y}\int_0^{L_x} L\,dx\,dy \\ &= -\pi a^2 w_x w_y\left[\sigma' - V_x\xi' - V_y\eta' + \frac{V_x^2}{2} + \frac{V_y^2}{2} - \frac{w_x^2 B'}{4} - \frac{w_y^2 C'}{4} - \frac{(w_x^2 - w_y^2)\Theta\phi'}{4}\right] \\ &- \frac{\pi a^2(w_x^2 + w_y^2)}{2w_x w_y}\left[1 + \frac{w_x^2 w_y^2\Theta^2}{4}\right] - \frac{1}{2}\pi a^2 w_x w_y(w_x^2 B^2 + w_y^2 C^2) + \sum_{n,m=1}^{\infty}\frac{\nu L_x L_y C_{nm}^2}{4\pi^2 Q_1}.\end{aligned} \tag{9}$$

Taking variations of the averaged Lagrangian (9) with respect to the elliptic nematicon parameters gives the variational, modulation equations, describing the evolution of the elliptic nematicon. These variational equations are detailed in Appendix A. The variational equations give only oscillatory solutions, since they are Hamiltonian, and do not evolve to a steady state. It has been well established [3, 41] that one must take into account the damping introduced by the diffractive radiation in order to reach the observed steady state. This interaction with the radiation has not been included in the chirp approximation. It was successfully included using the modulation theory method via the introduction of a shelf of diffractive radiation [41]. We thus examine the modulation equations including this shelf of radiation in the next section. In Section 5 we will show how the chirp trial function can be supplemented to account for the shed diffractive radiation. It will now be shown how the shelf approximation captures the effects of radiation on longer evolution scales.

3.2. Modulation Theory— Shelf of radiation

To account for diffractive radiation loss, Kath and Smyth [41] developed a new trial function that could be matched to the diffractive radiation shed by an evolving beam. The diffractive radiation loss itself was determined by solving the linearised equations for the (low amplitude) shed radiation. In this manner, solutions of the variational (modulation) equations found using this method could evolve to a steady state as $z \to \infty$, in agreement with numerical solutions. The new trial function is

$$E_s = \left[ae^{-(X^2/w_x^2+Y^2/w_y^2)} + ig\right] e^{i(\zeta+\zeta_s)}, \tag{10}$$

where a, w_x, w_y, X, Y and ζ have the same meaning as in section 3.1 for the chirp trial function. In this case, $\zeta_s = XY\Theta$, with Θ related to the OAM of the optical beam. This method differs from the chirp method as the trial function includes the extra term g, but omits the phase modulations B and C. This extra term is called a shelf, as it is independent of x and y. It arises as low wavenumber diffractive radiation and it has low group velocity, and so accumulates under the elliptic nematicon [3, 41]. This shelf term also allows matching to the diffractive radiation shed by the beam, introducing loss terms in the modulation equations, which allows the modulation solution to evolve to a steady state. A perturbation analysis of linearised governing equations of NLS-type has shown the existence of the shelf [41, 44]. It is also $\pi/2$ out of phase with the solitary wave as the in-phase component corresponds to changes in the amplitude and width of the solitary wave [3, 41]. The shelf of radiation that forms under the solitary wave cannot remain flat forever and must match to shed radiation. Hence, g is taken to be non-zero in the elliptically shaped region $w_y^2X^2 + w_x^2Y^2 \leq w_x^2w_y^2\ell^2$. The term ℓ gives the area of the shelf of radiation relative to that of the elliptic nematicon.

The trial function (10) and the Fourier series solution for the director angle (7), which is the same as that for the chirp trial function as $|E|^2$ is the same, are substituted into the Lagrangian (3), which is then averaged over the cell in the (x, y) plane, resulting in the averaged Lagrangian

$$\begin{aligned}\mathcal{L} = &-2\pi ag'w_xw_y + \frac{1}{4}\pi a^2w_xw_y\left(w_x^2 - w_y^2\right)\Theta\phi' + 2\pi a'gw_xw_y + 2\pi agw_x'w_y + 2\pi agw_xw_y' \\ &- \frac{\pi a^2w_y}{2w_x} - \frac{\pi a^2w_x}{2w_y} + \sum_{n,m=1}^{\infty}\frac{\nu L_xL_yC_{nm}^2}{4\pi^2Q_1} - \frac{1}{8}\pi a^2w_xw_y\left(w_x^2 + w_y^2\right)\Theta^2 \\ &- 4\pi\left(\frac{a^2w_xw_y}{4} + g^2\Lambda\right)\left(\sigma' - V_x\xi' - V_y\eta' + \frac{V_x^2}{2} + \frac{V_y^2}{2}\right).\end{aligned} \tag{11}$$

Here $\Lambda = \beta w_xw_y$, with β to be determined. The constant β is related to ℓ, which is determined by linearising the modulation equations about their steady state. This gives a harmonic oscillator equation whose frequency is matched to that of the steady nematicon [29, 41]. However, for nematicons in a finite cell, this linearisation process gives an equation which is too complicated to obtain sensible information from. In this case, it has been found easier to determine β by matching the frequency of oscillation of the solution of the modulation equations to that of the numerical solution for one choice of parameter values and verifying that this choice is robust over other choices of these parameters [22, 23]. The variational equations for the averaged Lagrangian (11), detailed in Appendix B, describe the evolution of the elliptical nematicon.

As discussed, the final parameter to be determined is the area of the radiation shelf, $\Lambda = \beta w_x w_y$. Comparisons with numerical solutions show that $\beta = 0.3$ gives good comparisons with full numerical solutions for a wide range of input beams.

The steady state for the elliptic nematicon can be found using total energy conservation for the system. Nöther's theorem is used to find the energy conservation equation based on the invariance of the Lagrangian (3) with respect to shifts in z, as z is a time-like variable. The averaged energy conservation equation is then given by

$$\begin{aligned}\frac{dH}{dz} &= \frac{d}{dz}\int_0^{L_y}\int_0^{L_x}\left[|\nabla E|^2 - 4\theta|E|^2 + \nu|\nabla\theta|^2\right]dx\,dy \\ &= \frac{d}{dz}\left\{\frac{\pi a^2 w_y}{2w_x} + \frac{\pi a^2 w_x}{2w_y} - \sum_{n,m=1}^{\infty}\frac{\nu L_x L_y C_{nm}^2}{4\pi^2 Q_1}\right\} = 0. \end{aligned} \tag{12}$$

The cell boundaries are found to be repulsive towards the nematicon [21–23, 39, 40]. As a result of this repulsion, the elliptic nematicon has a helical trajectory, spiralling towards the centre of the NLC cell, the final steady state position, due to momentum being shed to diffractive radiation. At the centre of the cell all four boundaries exert an equal amount of force on the nematicon, pinning it in place. The carat $\hat{}$ will be used to denote steady state values of the elliptic nematicon parameters. We then have $\hat{\xi} = L_x/2$, $\hat{\eta} = L_y/2$, $\hat{V}_x = 0$ and $\hat{V}_y = 0$. At the steady state the elliptic nematicon will have a circular cross-section due to symmetry. Hence, it will no longer be rotating with an orbital angular momentum and will have no discernible orientation angle due to its radial symmetry, so that $\hat{\Theta} = 0$ and $\hat{\phi} = 0$. Also, the elliptic nematicon will have stopped shedding radiation at its steady state, and hence the shelf height $\hat{g} = 0$. Thus, the modulation equation (B.8) can be used to find the steady state relationship between the amplitude $\hat{a}$ and width $\hat{w}$ of the steady state nematicon, as $\hat{w} = \hat{w}_x = \hat{w}_y$ at the steady state. This yields

$$\hat{a}^2 = \frac{4\nu L_x L_y}{\pi \hat{w}^6 \varpi}, \tag{13}$$

where

$$\varpi = \sum_{n,m=1}^{\infty} e^{-\hat{\gamma}_1}\sin\left(\frac{n\pi\hat{\xi}}{L_x}\right)\sin\left(\frac{m\pi\hat{\eta}}{L_y}\right), \quad \hat{\gamma}_1 = \frac{\pi^2\hat{w}^2 Q_1}{4}. \tag{14}$$

The combination of the energy conservation equation (12) and the steady state relation (13) is used to find the final steady state values for the amplitude and width of the elliptic soliton for given initial beam parameters.

Since solutions of a Hamiltonian system, such as the modulation equations, are only oscillatory, we need to add mass loss to diffractive radiation to obtain equations whose solutions evolve to a steady state. The mass loss is added as in previous work [22, 23, 29] using the mass flux calculated for the circular nematicon, but with a source which depends on the elliptical form of the shelf. The final equations are given in Appendix B. These equations will give the evolution to a steady state. However, there is an angular process which must be included in the approximation. It is observed from numerical solutions, see Figure 4, that as the ellipse rotates it sheds spiral wave radiation. In the early stages

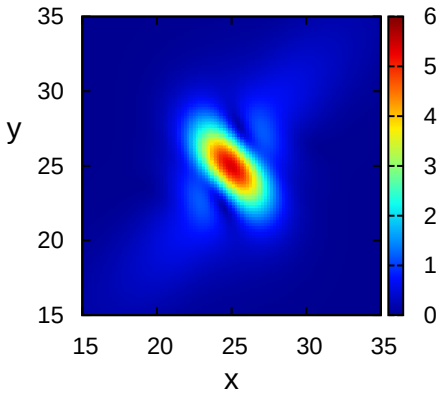

Figure 4: (Colour online) Profile of an elliptic nematicon rotating anti-clockwise with diffractive radiation shed along its major axis.

of the motion this loss is not important. However, as z increases the cumulative effect of this radiation decreases the angular velocity Ω. In the next section we shall calculate the effect of this spiral wave radiation.

3.3. Inclusion of angular momentum loss

As the elliptic nematicon evolves, it reshapes by shedding mass [45], that is optical power, to become circular over large z distances. This reshaping is a consequence of the symmetry of the medium [10, 11]. In addition, the reshaping is driven by loss of angular momentum to shed diffractive radiation. By overall conservation of angular momentum, as the elliptic nematicon loses angular momentum, its angular velocity slows. The net result is that the elliptic nematicon becomes circular, so that $w_y \to w_x$ as $z \to \infty$.

It is clear that it is necessary to determine the angular momentum shed by the nematicon to diffractive radiation as it evolves. Due to the spinning of the beam, these shed waves have a spiral pattern. As the spiral waves [46] have small amplitude relative to the beam, it can be seen from the electric field equation (1) that they satisfy Schrödinger's equation

$$iE_z + \frac{1}{2}\nabla^2 E = 0. \tag{15}$$

The boundary condition for these spiral waves at the elliptic nematicon is a signalling boundary condition as the elliptic beam shelf sheds the spiral waves. To determine this boundary condition, recall that the trial function for the elliptic nematicon is (10), which is in the rotating frame of reference, with coordinates and angular velocity given by (B.6). As the radiation matches to the edge of the shelf, matching to the shelf term in the trial function (10) yields

$$E = ige^{i(\sigma+\Theta XY)} \tag{16}$$

at the edge of the shelf $w_y^2X^2 + w_x^2Y^2 \leq w_x^2w_y^2\ell^2$. For ease in notation and calculation,

the rotating coordinates X and Y can be written in matrix form

$$\begin{pmatrix} X \\ Y \end{pmatrix} = A(\phi) \begin{pmatrix} x \\ y \end{pmatrix}, \tag{17}$$

where the rotation matrix is

$$A(\phi) = \begin{pmatrix} \cos\phi & \sin\phi \\ -\sin\phi & \cos\phi \end{pmatrix}. \tag{18}$$

The coordinate transform (17) can be inverted to give

$$\mathbf{x} = \begin{pmatrix} x \\ y \end{pmatrix} = A^{-1}(\phi) \begin{pmatrix} pw_x \cos\mu \\ pw_y \sin\mu \end{pmatrix}. \tag{19}$$

The level lines of the shelf trial function (10) are ellipses parametrised in the form

$$X(\mu) = pw_x \cos\mu \quad \text{and} \quad Y(\mu) = pw_y \sin\mu, \tag{20}$$

where $0 \leq \mu \leq 2\pi$ and p is to be chosen later. The real function g has an amplitude given by $\bar{g}$ and frequency $\sigma(z)$. Thus the product in (16) has two terms. The first one with a $2\sigma(z)$ in the phase and the second with only the μ dependent term. The term containing the $2\sigma(z)$ in (16) contributes to a symmetric wave since the angular term is smaller. Hence, it is the second term that contributes to the spiral waves. It takes the form

$$E = i\frac{\bar{g}}{2} \exp[i\Theta(z)p^2 w_x w_y \cos\mu \sin\mu] \tag{21}$$

on applying the signalling boundary condition on the curve (19).

The radiation equation (15) will be solved using a geometric optics solution [24] with

$$E = ue^{iS(x,y,z)}, \tag{22}$$

to leading order. Substituting this solution form into the radiation equation (15) yields the eikonal equation

$$S_z + \frac{1}{2}|\nabla S|^2 = 0. \tag{23}$$

Applying the boundary condition (21), we have that

$$S(x, y, z) = \Theta(z)p^2 w_x w_y \cos\mu \sin\mu \tag{24}$$

and $u = \bar{g}/2$ on the moving boundary given by equation (19).

To find the angular momentum radiated by the elliptic nematicon, we need to determine the derivative of S normal to the boundary curve at the elliptic shelf. To obtain this derivative, the eikonal equation (23) is rewritten using the tangential coordinate μ and the normal coordinate λ of the elliptical boundary (19) in the form

$$\begin{pmatrix} x \\ y \end{pmatrix} = \mathbf{X} = +\lambda \mathbf{n}(z, \mu), \tag{25}$$

where

$$\mathbf{X} = \begin{pmatrix} X(\mu) \\ Y(\mu) \end{pmatrix}, \tag{26}$$

$$\mathbf{n} = \frac{\mathbf{X}_\mu^\perp}{|\mathbf{X}_\mu|} = \frac{1}{|\mathbf{X}_\mu|} \begin{pmatrix} -y_\mu \\ x_\mu \end{pmatrix}. \tag{27}$$

Here, X_μ and Y_μ are given by

$$\begin{pmatrix} -Y_\mu \\ X_\mu \end{pmatrix} = A^{-1}(\phi) \begin{pmatrix} -pw_x \cos\mu \\ pw_y \sin\mu \end{pmatrix}. \tag{28}$$

The norm of $\mathbf{X}_\mu^\perp$ is equal to the norm of $\mathbf{X}_\mu$ and is

$$|\mathbf{X}_\mu| = p\sqrt{w_x^2 \sin^2\mu + w_y^2 \cos^2\mu}\,. \tag{29}$$

In these coordinates, the eikonal equation (23) becomes

$$S_z + \frac{1}{2}\left\{ \left(\frac{S_\mu}{|\mathbf{X}_\mu|} \right)^2 + S_\lambda^2 \right\} = 0, \tag{30}$$

where S_μ and S_λ are the derivatives of S with respect to μ and λ respectively. To obtain the flux at the boundary it is not necessary to find the full solution of (30). We only require the value of S_λ at the boundary of the ellipse $\lambda = 0$. Since the boundary is moving, we obtain

$$S_z + \nabla S \cdot \mathbf{X}_z = \frac{1}{2}\Theta_z p^2 w_x w_y \sin(2\mu) + \sigma_z. \tag{31}$$

In this calculation, the derivatives on the slowly varying axes w_x and w_y have been neglected. This relates the z derivative S_z to the boundary condition and the spatial derivative. To obtain the desired expression, we note that

$$\begin{aligned} \nabla S \cdot \mathbf{X}_z &= \frac{S_\mu}{|\mathbf{X}_\mu|^2}\left(\mathbf{X}_\mu \cdot \mathbf{X}_z\right) + \frac{S_\lambda}{|\mathbf{X}_\mu|}\left(\mathbf{X}_\mu^\perp \cdot \mathbf{X}_z\right) \\ &= \phi_z p^2 \left[\frac{w_x w_y S_\mu}{|\mathbf{X}_\mu|^2} + \frac{(w_x^2 + w_y^2)\sin(2\mu)\, S_\lambda}{2\,|\mathbf{X}_\mu|} \right]. \end{aligned} \tag{32}$$

Then from equation (31) we obtain

$$S_z = \frac{1}{2}\Theta_z p^2 w_x w_y \sin(2\mu) + \sigma_z - \phi_z p^2 \left[\frac{w_x w_y S_\mu}{|\mathbf{X}_\mu|^2} + \frac{(w_x^2 + w_y^2)\sin(2\mu)\, S_\lambda}{2\,[\mathbf{X}_\mu|} \right]. \tag{33}$$

Substitution of this expression into the eikonal equation (30) gives

$$\begin{aligned} &\frac{1}{2}\Theta_z p^2 w_x w_y \sin(2\mu) + \sigma_z + \frac{1}{2}\left[\left(\frac{S_\mu}{|\mathbf{X}_\mu|} \right)^2 + S_\lambda^2 \right] \\ &- \phi_z p^2 \left[\frac{w_x w_y S_\mu}{|\mathbf{X}_\mu|^2} + \frac{(w_x^2 + w_y^2)\sin(2\mu)\, S_\lambda}{2\,|\mathbf{X}_\mu|} \right] = 0 \end{aligned} \tag{34}$$

as the equation for S_λ on the boundary.

Now ϕ_z can be replaced using the modulation equation (B.6) and S_μ is given by the derivative of the boundary condition (24) with respect to μ, to yield

$$S_\mu = \Theta p^2 w_x w_y \cos(2\mu), \tag{35}$$

as σ is a function of z only.

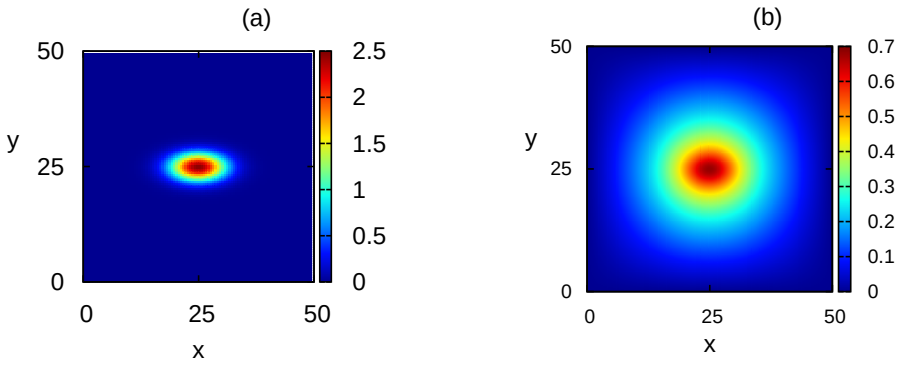

Figure 5: (Colour online) Input (a) elliptic soliton $|E|$ and (b) the corresponding NLC distribution θ. The NLC distribution is smoothed due to the nonlocality of the medium, resulting in a circular cross-section as opposed to mimicking the cross-section of the elliptic soliton. The initial parameter values are $a = 2.5$, $w_x = 6$, $w_y = 3$, $\phi = 0$, $\Theta = 0.07593$, $(\xi, \eta) = (25, 25)$ and $(V_x, V_y) = (0, 0)$, with $\nu = 200$ and $(L_x, L_y) = (50, 50)$.

Furthermore, numerical simulations indicate that the radiation shed by the elliptic nematicon occurs mainly long the major axis, as shown in Figure 4. Thus, the angle at which radiation is shed is small, leading to the approximations $\cos(2\mu) \approx 1$ and $\sin(2\mu) \approx 0$. Now, equation (34) can be re-expressed as a quadratic equation for the derivative normal to the boundary curve, S_λ in the form

$$-\frac{\Theta^2 p^4 w_x^2 w_y^2 (w_x^2 + w_y^2)}{(w_x^2 - w_y^2)\left|\mathbf{X}_\mu\right|^2} + \frac{\Theta^2 p^4 w_x^2 w_y^2}{2\left|\mathbf{X}_\mu\right|^2} + \frac{S_\lambda^2}{2} = 0. \tag{36}$$

Solving equation (36) results in the derivative of the normal to the boundary curve as

$$S_\lambda = \frac{\Theta p w_x \sqrt{w_x^2 + 3w_y^2}}{(w_x^2 - w_y^2)^{1/2}}. \tag{37}$$

This equation will be shown to determine the flux of radiation.

To determine the angular momentum radiation damping we consider the angular momentum balance in the form

$$\frac{d}{dz}\iint_\Omega (\mathbf{X} \times \nabla E) \cdot E^* dx\, dy = 2\,\mathbf{Re}\int_C (\nabla E \cdot \mathbf{n})(\nabla E^* \times \mathbf{X})\, dl. \tag{38}$$

Using for the contour C the shelf boundary, we obtain for the flux

$$F = 2\,\mathbf{Re}\int_0^{2\pi} (\nabla E\cdot\mathbf{n})\,(\nabla E^*\times\mathbf{X})\,|\mathbf{X}_\mu|\,d\mu. \tag{39}$$

Using the geometric optics solution for E given by equation (22), the angular momentum flux can be rewritten in terms of the tangential and normal coordinates as

$$\begin{aligned} F &= 2\,\mathbf{Re}\int_0^{2\pi} (iue^{iS}S_\lambda)\left[-iue^{-iS}\left(\frac{S_\mu}{|\mathbf{X}_\mu|^2}(\mathbf{X}_\mu\times\mathbf{X})+\frac{S_\lambda}{|\mathbf{X}_\mu|}(\mathbf{X}_\mu^\perp\times\mathbf{X})\right)\right]d\mu \\ &= 2\,\mathbf{Re}\,\frac{\partial}{\partial z}\int_0^{2\pi}\left[u^2S_\lambda\left(\frac{S_\mu}{|\mathbf{X}_\mu|^2}(\mathbf{X}_\mu\times\mathbf{X})+\frac{S_\lambda}{|\mathbf{X}_\mu|}(\mathbf{X}_\mu^\perp\times\mathbf{X})\right)\right]d\mu. \end{aligned} \tag{40}$$

Here

$$\mathbf{X}_\mu\times\mathbf{X} = -p^2w_xw_y\begin{pmatrix}\sin\mu\\ \cos\mu\end{pmatrix}\sim -p^2w_xw_y, \tag{41}$$

$$\mathbf{X}_\mu^\perp\times\mathbf{X} = -\frac{1}{2}p^2\begin{pmatrix}w_x^2\sin(2\mu)\\ w_y^2\sin(2\mu)\end{pmatrix}\sim 0, \tag{42}$$

using the small angle approximation for μ. The norm under the small angle approximation for μ is given by $|\mathbf{X}_\mu|^2 = p^2(w_x^2\sin^2\mu + w_y^2\cos^2\mu)\sim p^2w_y^2$. This final contribution to the angular momentum flux, using the same small angle approximation for μ as before, results in the angular momentum flux to radiation

$$\begin{aligned} F &= -2\,\mathbf{Re}\int_0^{2\pi}\frac{u^2p^2w_xw_yS_\lambda S_\mu}{|\mathbf{X}_\mu|}\,d\mu \\ &= -2\,\mathbf{Re}\int_0^{2\pi}\frac{u^2\Theta^2p^4w_x^3w_y\sqrt{w_x^2+3w_y^2}}{(w_x^2-w_y^2)^{1/2}}\,d\mu. \end{aligned} \tag{43}$$

A more robust choice for the average amplitude $\bar{g}/2$ of the shelf is to estimate the shelf height by the mass difference between the revolving nematicon and the final state. We thus take $u\sim\Gamma\kappa\sqrt{\hat{\Lambda}}$, with κ given by (B.15). $\Gamma = 0.3$ was found to be a robust choice to give good comparisons with full numerical solutions. The parametrisation variable p was set to equal one. This assumes, in agreement with numerical results, that the shelf is attached to the nematicon.

The calculated angular momentum flux loss must now be added to the modulation equation related to the angular momentum of the elliptic soliton, equation (B.7). Doing this yields

$$\begin{aligned} \frac{d}{dz}\left[a^2w_xw_y\left(w_x^2-w_y^2\right)\Theta\right] &= -\frac{u^2\Theta^2p^4w_x^3w_y\sqrt{w_x^2+3w_y}}{(w_x^2-w_y^2)^{1/2}} \\ &+\sum_{n,m=1}^{\infty}\frac{2\pi a^4w_x^2w_y^2\alpha e^{-\gamma_1}}{\nu L_xL_yQ_1\rho_1}\left[\frac{n\cos(2\phi)\left(w_x^2-w_y^2\right)G}{L_x}-\frac{\alpha M\rho_3}{\rho_1}\right]. \end{aligned} \tag{44}$$

The modulation equations (B.1) to (B.6), (B.8), (B.9), plus equation (44), as well as the algebraic equation (B.10) form a system of first-order ODEs for the evolution of the elliptic nematicon which include both mass and angular momentum losses to dispersive radiation. We remark that the matching of the spiral wave is achieved using the shelf trial function (10). We thus expect that an appropriate understanding of the shelf behaviour during rotation is needed to obtain a good approximation to the elliptic beam evolution. We will show later that the behaviour of the shelf determines an evolution on two different time scales and that the inclusion of angular momentum loss is vital to obtain good comparisons of solutions of the modulation equations with full numerical solutions.

4. Shelf solution— Results

In this section, we shall compare full numerical solutions of the nematicon equations (1) and (2) which govern the propagation of an elliptic nematicon through a finite sized NLC cell with solutions of the modulation equations of Section 3. These approximate equations were derived using modulation theory including radiation loss (shelf method) and, finally, including both radiation and angular momentum loss, the details of which can be found in sections 3.2 and 3.3, respectively.

The variational equations listed in Appendix A and Appendix B were solved using the standard fourth order Runge–Kutta method. The full numerical solution of the electric field equation (1) was found using second order centred differences for the Laplacian $\nabla^2 E$ and a second order predictor-corrector method, based on the second order Runge-Kutta method, to advance forward in z, the propagation direction. The director equation (2) was solved using centred second order differences for the Laplacian $\nabla^2\theta$ and Jacobi iteration to solve the resulting linear system. The initial condition for the envelope of the electric field in the numerical simulations was the trial function equation (10), at $z = 0$ and $g = 0$. Hence, the initial condition for the optical beam is

$$E = ae^{-(X^2/w_x^2+Y^2/w_y^2)}e^{i(\zeta+\Theta XY)}. \tag{45}$$

To maintain the accuracy and stability of the full numerical scheme, the step sizes used were $\Delta x = \Delta y = 0.2$ and $\Delta z = 0.001$. The propagation length was taken to be $z = 500$, a typical non-dimensional cell length [34]. The numerical investigation was conducted using several different cell sizes with various non-dimensional widths, $50 \leq L_x \leq 100$ and $50 \leq L_y \leq 100$.

Let us first consider a propagating elliptical nematicon initially positioned in the centre of a square NLC cell, with a non-dimensional width and breadth of $(L_x, L_y) = (50, 50)$. This initial elliptical beam is illustrated in Figure 5(a), with the corresponding director distribution shown in Figure 5(b). The nonlocal response of the director to the elliptical optical beam has smoothed the director distribution, resulting in it having a circular cross section, rather than following the elliptical beam cross section. The response of the director to the elliptical beam allows the formation of an elliptical nematicon by balancing the diffractive spreading of the optical beam with the induced self-focusing due to the nonlinear dependence of the refractive index of the NLC on the beam intensity [1, 38].

The corresponding evolution plots for the stationary elliptic soliton with OAM are shown in Figure 3, where it can be seen that the elliptic soliton stably propagates within

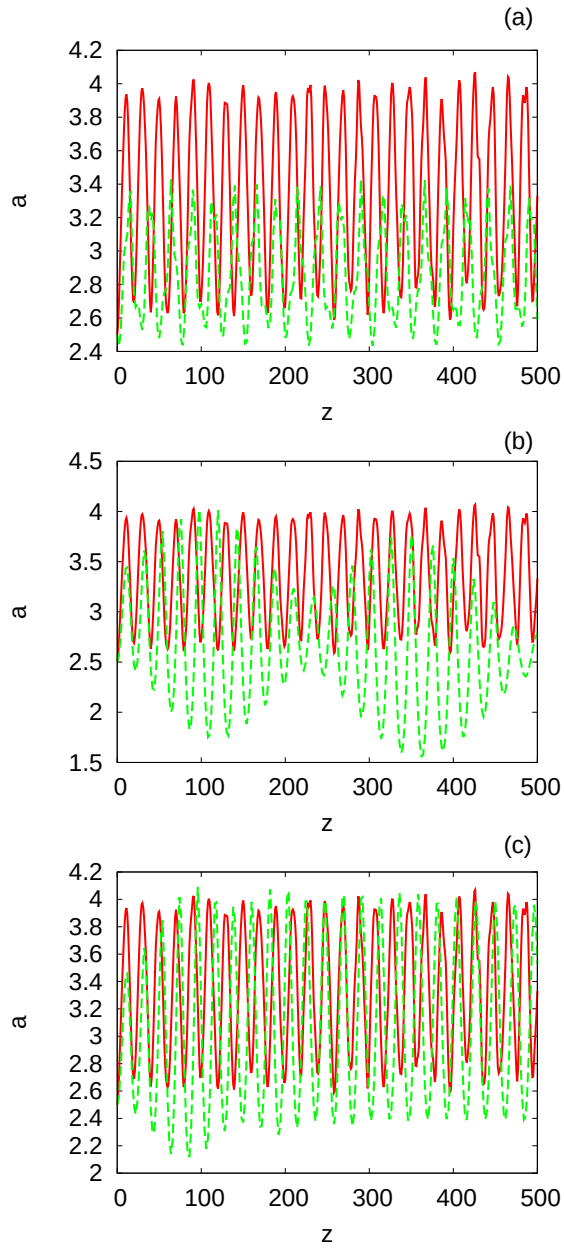

Figure 6: (Colour online) Amplitude a as given by the full numerical solution (red solid line) and (a) chirp method solution (green dashed line), (b) modulation theory solution including radiation mass loss (green dashed line), and (c) modulation theory solution including radiation mass loss and angular momentum loss (green dashed line). The initial values are $a = 2.5$, $w_x = 6$, $w_y = 3$, $\phi = 0$, $\Theta = 0.07593$, $(\xi, \eta) = (25, 25)$ and $(V_x, V_y) = (0, 0)$, with $\nu = 200$ and $(L_x, L_y) = (50, 50)$.

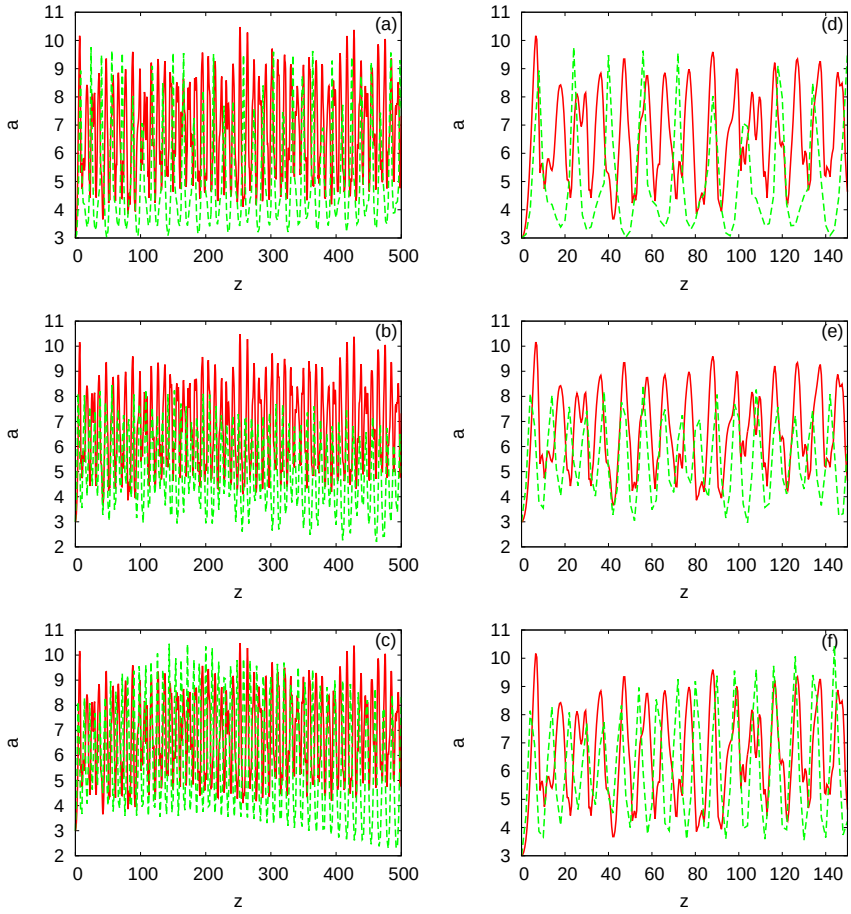

Figure 7: (Colour online) Amplitude a as given by the full numerical solution (red solid line) and (a) chirp method solution (green dashed line), (b) modulation theory solution including radiation mass loss (green dashed line), (c) modulation theory solution including radiation mass loss and angular momentum loss (green dashed line) and the full numerical solution (red solid line) and (d) chirp method solution (green dashed line), (e) modulation theory solution including radiation mass loss (green dashed line), (f) and modulation theory solution including radiation mass loss and angular momentum loss (green dashed line) for a reduced z length. The initial values are $a = 3$, $w_x = 7$, $w_y = 4$, $\phi = 0$, $\Theta = 0.06194$, $(\xi, \eta) = (25, 25)$, and $(V_x, V_y) = (0, 0)$, with $\nu = 200$ and $(L_x, L_y) = (50, 50)$.

the NLC cell. The rotation caused by the addition of OAM can be seen in the phase plots. Figure 3(e) suggests a possibility of instability. However, this is not the case as there is only one peak and the shelf of radiation that is evolving under the elliptic soliton [41] is reshaping to shed radiation via angular momentum loss (see Section 3.3).

We are interested in comparisons of the modulation theory solutions with the full numerical results and solutions of the chirp equations of Appendix A to determine the relative accuracy and applicability of the various approximate methods. An amplitude comparison is shown in Figure 6 for a typical input beam. Due to the optical beam's initial position in the centre of the cell, the position of the elliptical nematicon does not change during propagation. Hence, there is no non-trivial position information to compare. From Figure 6 we can see that both the chirp solution and the modulation theory solution including radiation mass loss give amplitudes which oscillate around a different mean to that of the full numerical solution. However, the modulation theory solution including radiation mass loss has the same oscillation period as that of the full numerical solution and has a similar envelope decay rate to that of the numerical solution. Including both radiation mass loss and angular momentum loss to the modulation equations results in the modulation solution oscillating about the same mean (final state) as the full numerical solution. This shows the key role which angular momentum loss plays in the evolution of the elliptical nematicon. Furthermore, the modulation theory solution including radiation mass loss displays signs of beating, which is no longer present when angular momentum loss is added to the equations. Lastly, it can be seen that the chirp method does not provide an adequate approximation as loss, both mass and angular momentum, is not incorporated using this method. We will consider later the coupling of radiation to the chirp solution.

Figure 7(a) shows an amplitude comparison for the chirp method for a different input beam positioned in the centre of the NLC cell. It can be seen that the chirp solution does not have the same period as that of full numerical solution, but that both modulation solutions, shown in Figures 7(b) and (c), do. In Figures 7(d)–(f) the initial stages of the full evolution of the solutions are shown, $0 \leq z \leq 150$, so that the details of the comparisons between the different variational solutions and the numerical solution can be clearly seen. The chirp solution's oscillation is not in agreement with that of the full numerical solution, although the amplitude evolution is within the correct envelope. Radiation mass loss added to the modulation theory equations causes the amplitude oscillation to pick up an extra frequency, resulting in beating, as was seen in Figure 6(b) and Figure 7(b). However, the period of the amplitude oscillation is in excellent agreement with that of the full numerical solution. This shows that the choice in Section 3.2 of the parameter β, which is related to the area of the shelf of low wavenumber radiation under the nematicon, is robust. When angular momentum loss is included in the modulation equations, the beating is lost, as for the solution shown in Figure 6, with the oscillation period still being in excellent agreement with that of the numerical solution. There is now good overall agreement with the full numerical solution. It should be noted that the numerical solution shows evidence of a second period due, most likely, to the independent oscillations of the two axes of the ellipse.

Figure 8 shows a comparison between the full numerical solution of the nematicon equations, the solution of the chirp equations and the solution of the modulation equations which include the solution with and without angular momentum loss, for a case in which the beam is off centre, so that it propagates around the cell as it evolves. As in

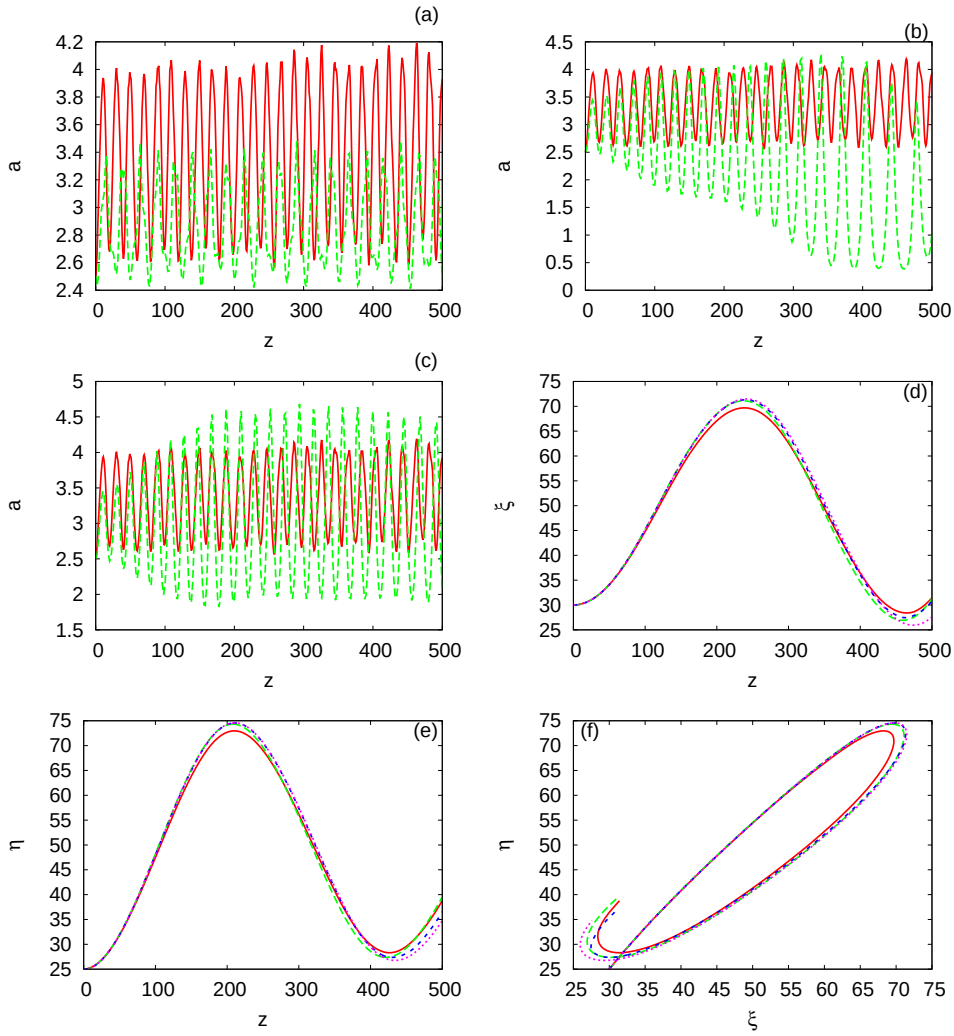

Figure 8: (Colour online) Comparison between the full numerical solution (red solid line) and (a) chirp method solution (green dashed line), (b) modulation theory solution including radiation mass loss (green dashed line) and (c) modulation theory solution including radiation mass loss and angular momentum loss (green dashed line) for amplitude a. A comparison between the full numerical solution (red solid line) and chirp method solution (green dashed line), modulation theory solution including radiation mass loss (blue short dashed line), modulation theory solution including radiation mass loss and momentum loss (magenta dotted line) for (d) x position (e) y position and (f) (x, y) position for a square cell. The initial values are $a = 2.5$, $w_x = 6$, $w_y = 3$, $\phi = 0$, $\Theta = 0.06194$, $(\xi, \eta) = (30, 25)$, and $(V_x, V_y) = (0, 0)$, with $\nu = 200$ and $(L_x, L_y) = (100, 100)$.

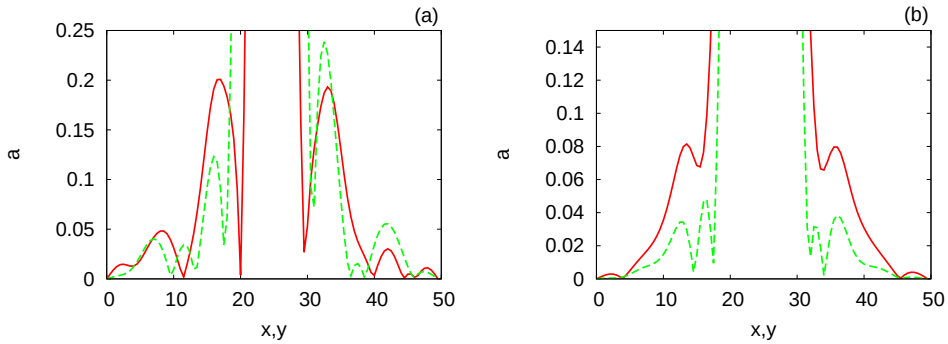

Figure 9: (Colour online) The full numerical solution for elliptic beams depicting the cross section of the ellipse at $x = 25$ (solid red line) and $y = 25$ (green dashed line). The profile (a) shows an elliptic beam with a large initial ellipticity. The solution is not near the steady state, as shown by the amount of radiation. The shed radiation humps in both directions are non-symmetric. Profile (b) is for an elliptic beam with a small initial ellipticity (almost circular). The beam is radiating less and the shed radiation humps are symmetric. The initial values of the width are (a) $w_x = 6$, $w_y = 3$ and (b) $w_x = 4$, $w_y = 3$. The remaining initial values are $a = 2.5$, $\phi = 0$, $\Theta = 0.06194$, $(\xi, \eta) = (30, 25)$ and $(V_x, V_y) = (0, 0)$, with $\nu = 200$ and $(L_x, L_y) = (100, 100)$.

previous studies [22, 23, 39, 40], the walls of the cell repel the nematicon. The amplitude comparison is similar to that of Figures 6 and 7, for which the nematicon was stationary in the centre of the cell. It can be seen that the inclusion of angular momentum loss to radiation is vital in order to obtain agreement with the numerical solution, with this loss driving the evolution of the nematicon. Figure 8(c) shows a larger decrease in the amplitude in comparison with the full numerical solution. The reason for this difference is that the mass loss calculation is an approximation to the actual mass loss and in this case, and that shown in Figure 7(c), gives a mass loss which is too large. Figures 8(d)–(f) show excellent comparisons for the elliptic nematicon's trajectory, with little difference between the various variational solutions. This is because the amplitude and width evolution decouple from the position and velocity oscillations of nonlinear beams in NLC, as found in previous work [27, 33, 47, 48]. Figure 8(f) shows the helical trajectory of the beam down the z direction, which is into the page, in agreement with the trajectories found for nematicons and optical vortices in previous studies [22, 23, 39, 40]. This is again due to the repulsive effect of the walls on the nematicon [22, 23, 39, 40].

5. Chirp radiation coupling

In order to couple the angular momentum loss to the chirp equations we need to provide a matching condition for the spiral waves. In the shelf approximation this was provided by the shelf height g which was determined by the mass difference between the evolving elliptic nematicon and the steady circular nematicon.

To determine a matching between the chirp solution and the radiation we use the argument of Kath and Smyth [41]. We expand the chirp trial function in the form, assuming that B and C are small,

$$E_c = a e^{-X^2/w_x^2 - Y^2/w_y^2} e^{i(\Theta XY + \sigma)} \left\{1 + iBX^2 + iCY^2\right\}. \tag{46}$$

We can now interpret the term

$$\left(iBX^2e^{-X^2/w_x^2-Y^2/w_y^2}+iCY^2e^{-X^2/w_x^2-Y^2/w_y^2}\right)e^{i\sigma}, \tag{47}$$

as the sum of two shelves, one along X with amplitude B and the other along Y with amplitude C. They have a similar behaviour to that discussed in the 1 dimensional case [44] and must be related to a Jordan block of the linearisation around the nematicon solution. From the nematicon solution we observe that the radiation does have a hump-like behaviour, such as the one of equation (47), see Figure 9. Figure 9(a) shows that the radiation forms humps on either side of the evolving elliptic nematicon. These humps are non-symmetric and indicate that the beam is shedding large amounts of diffractive radiation and angular momentum as compared with the case shown in Figure 9(b). Figure 9(b) depicts an elliptic beam with a more uniform circular cross-section. In this case the radiation humps hug the beam and are symmetric. This evolution indicates that in the initial stages the chirp solution captures the shelf structure and provides an appropriate boundary condition for the radiation. As the elliptical shape is lost, however, it no longer provides the mass loss of the shelf in the form of circular radiation. We will show that the shelf approximation gives better agreement with numerical solutions than the chirp method when supplemented by angular momentum loss.

To complete the trial function we just leave the widths w_x and w_y to be replaced by two new parameters in the shelf, which we take to be λ_x and λ_y. In order to match with the radiation we assume that the radiation is generated at the humps. Then the integral in (40) is approximated by taking the average value at the maxima to give

$$F_c=-2\,\mathbf{Re}\int_0^{2\pi}\frac{u_c^2\Theta^2w_x^3w_y\sqrt{w_x^2+3w_y^2}}{2e(w_x^2-w_y^2)^{1/2}}\,d\mu \tag{48}$$

for the flux, where $u_c\sim\lambda_x\lambda_y\kappa_c$. κ_c is given by (50) and $\lambda_x\lambda_y=0.05$, which was found to be a consistent match with full numerical solutions.

The decay of mass in the chirp approximation is then given by

$$\delta_c=-\frac{(2\pi)^{\frac{3}{2}}(\lambda_x\lambda_y)^4\kappa_c^2}{16e^3}\int_0^z\kappa_c(z')\ln[(z-z')/\tilde{\Lambda}_c^2]\frac{dz'}{(z-z')}\times \left[\left(\left\{\frac{1}{2}\ln[(z-z')/\tilde{\Lambda}_c^2]\right\}^2\frac{3\pi^2}{4}\right)^2+\pi^2\left\{\ln[(z-z')/\tilde{\Lambda}_c^2]\right\}^2\right]^{-1}, \tag{49}$$

where

$$\kappa_c^2=a(w_x^2B+w_y^2C) \tag{50}$$

$$\tilde{\Lambda}_c=\frac{w_x+w_y}{2} \tag{51}$$

It is to be noted that the free parameter $\lambda_x\lambda_y$ now plays the role of β. It is a measure of the distance between the shelf and the core of the elliptic nematicon. The mass loss can now be added in a similar manner as for the modulation equations to obtain instead

(b)

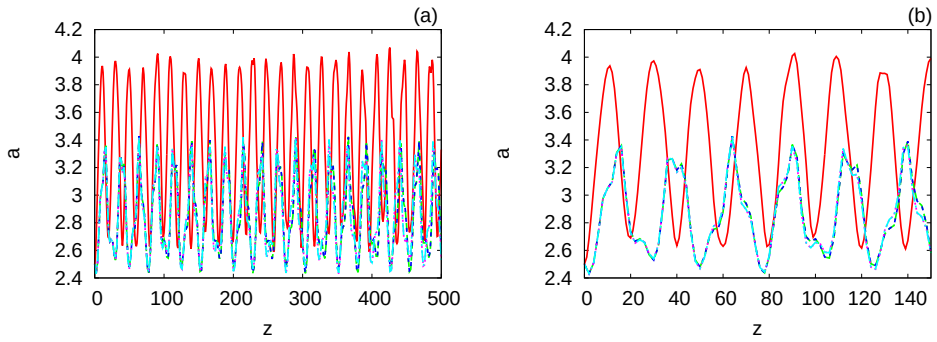

Figure 10: (Colour online) Comparison between the full numerical solution (red solid line) and chirp solution (green dashed line), the chirp solution including mass loss only (blue dot-dashed line), the chirp solution including angular momentum loss only (magenta dotted-line) and the chirp solution including both mass and angular momentum loss (light blue dot-long dashed line) for (a) the amplitude a and (b) for the amplitude a for the reduced propagation length z. The initial values are $a = 2.5$, $w_x = 6$, $w_y = 3$, $\phi = 0$, $\Theta = 0.07593$, $(\xi, \eta) = (25, 25)$ and $(V_x, V_y) = (0, 0)$, with $\nu = 200$ and $(L_x, L_y) = (50, 50)$.

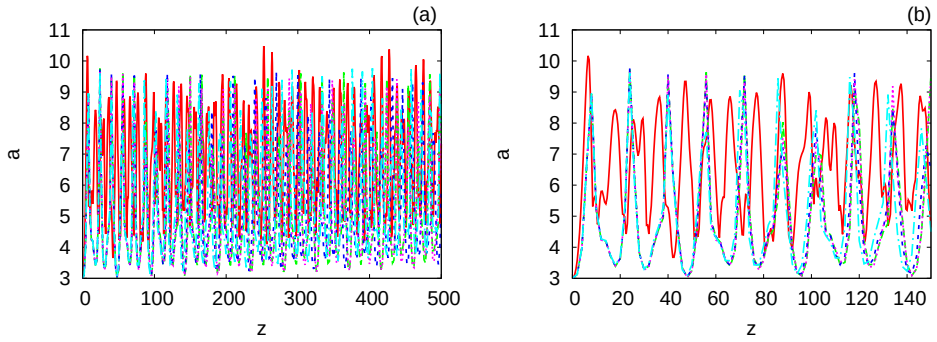

Figure 11: (Colour online) Comparison between the full numerical solution (red solid line) and chirp solution (green dashed line), the chirp solution including mass loss only (blue dot-dashed line), the chirp solution including angular momentum loss only (magenta dotted-line) and the chirp solution including both mass and angular momentum loss (light blue dot-long dashed line) for (a) the amplitude a and (b) for the amplitude a for the a reduced propagation length z.. The initial values are $a = 3$, $w_x = 7$, $w_y = 4$, $\phi = 0$, $\Theta = 0.06194$, $(\xi, \eta) = (50, 50)$ and $(V_x, V_y) = (0, 0)$, with $\nu = 200$ and $(L_x, L_y) = (100, 100)$.

of the mass equation (A.1) the new equation

$$\frac{d}{dz}\left[a^2 w_x w_y\right] = -2\delta_c \tilde{\Lambda}_c \kappa_c^2, \tag{52}$$

The equation governing angular momentum loss (A.8) becomes

$$\begin{aligned}\frac{d}{dz}\left[a^2 w_x w_y (w_x^2 - w_y^2)\Theta\right] = &\sum_{n,m=1}^{\infty} \frac{2\pi a^4 w_x^2 w_y^2 \alpha e^{-2\gamma_1}}{\nu L_x L_y \rho_1 Q_1}\left[\chi - \frac{\alpha M \rho_3}{\rho_1}\right] \\ &- \frac{u_c^2 \Theta^2 w_x^3 w_y \sqrt{w_x^2 + 3w_y^2}}{2e(w_x^2 - w_y^2)}.\end{aligned} \tag{53}$$

These equations, along with equations (A.2) to (A.7) and (A.9) to (A.13), form the complete set of approximate equations governing the evolution of an elliptic nematicon under the chirp method and include mass and angular momentum losses. It is to be noted that due to the nature of the trial function, the variational equations become linearly dependent as $\Omega \to 0$, since $w_y \to w_x$. For this reason we do not expect good agreement for the improved equations as the elliptic nematicon becomes circular. This lack of agreement is related to the fact that the shelf loses its hump-like structure as it becomes circular, as shown in Figure 9. In this case the radiation hugs the core and becomes more symmetric.

Figures 10 and 11 show a comparison between the modified chirp solution and the full numerical solution. The figures show that the modified chirp solution compares well with the numerical solution, provided the nematicon is elliptic. However, as expected, the comparison deteriorates as the nematicon becomes circular around $z = 200$. This is due to the change of the radiation shelf, which is not captured by our approximation. It must also be noted that omitting the mass loss from the chirp equations does not affect the solution. We conclude that the evolution of the nematicon from elliptic to circular is dominated by angular momentum loss. The shelf modulation solution shows a much better comparison in the almost circular phase. This is caused by the mass loss which, by construction, drives the nematicon to the steady state. In the chirp solution with radiation this is not present. We thus conclude that the second phase of the evolution is dominated by mass loss. These observations also show that for the angular momentum radiation, a detailed knowledge of the driving amplitude is not needed to calculate the angular momentum loss.

6. Conclusions

The evolution of elliptical nematicons with OAM in finite sized NLC cells has been studied for large propagation distances, corresponding to a large number of rotations of the beam. The dominating effect of angular momentum loss to the diffractive radiation shed by the elliptic nematicon as it evolves as been demonstrated, an effect which was not considered in previous work on elliptical solitary waves, as this previous work studied the beam evolution for small propagation distances and number of revolutions [13, 49]. We have shown that during the first part of the evolution the radiation of spiral waves stops the spinning, making the nematicon more circular. After this, mass loss becomes important and drives the nematicon to the final steady circular, non-spinning state.

As there are no known solitary wave solutions of the equations governing nonlinear beam propagation in a nematic liquid crystal, a semi-analytical approach based on an exact solution, derived using Fourier series, of the elliptic equation governing the director distribution and a variational solution of the beam equation, based on trial functions, for the beam profile was used. The approximate solution with a shelf trial function suitably modified to account for the ellipticity of the beam provides a very good approximation, provided the angular momentum shed to spiral waves is taken into account as radiation damping. It is to be remarked that the geometric optics approximation provides a very good approximation for the outgoing flux since it accurately captures the streaming of waves produced as the beam rotates.

We also show how angular momentum damping can be added to the chirp solution to obtain a good comparison when the beam is elliptic. As the beam becomes more circular, however, this approximation breaks down since the shape of the radiation shelf is no longer close to the assumed dependence in the modified chirp trial function.

Finally, we identified two stages in the evolution. The early one, which is dominated by angular momentum loss, and the final stage, which is dominated by mass loss. We found that the shelf solution with angular momentum loss gives a uniform approximation (in z), since the angular momentum shedding is not very sensitive to the shape of the radiation around the core of the nematicon. It also correctly captures the mass loss during the latter stages of the motion. It is to be remarked that the variational approximations coupled with approximate radiation damping are capable of displaying in quantitative detail the mechanisms involved in this nonlinear, nonlocal process. Finally, since the equations for the trajectory of the beam are dominated by the repulsion of the walls and are only weakly coupled to the elliptic soliton parameters, both the chirp and shelf methods give very good comparisons with numerical solutions.

N.F. Smyth acknowledges support by the Royal Society of London under grant IE111560. L.W. Sciberras acknowledges support from the postdoctoral fellowship program DGAPA-UNAM, Mexico. The authors thank the referees for their insightful comments which have greatly improved the presentation of this paper.

Appendix A. Variational Equations: Chirp

The variational equations derived by taking variations of the averaged Lagrangian (9) for the parameters of the chirped trial function (6) are

$$\frac{d}{dz}\left[a^2 w_x w_y\right] = 0, \tag{A.1}$$

$$\frac{d\xi}{dz} = V_x, \qquad \frac{d\eta}{dz} = V_y, \tag{A.2}$$

$$\frac{d}{dz}\left[a^2 w_x w_y V_x\right] = -\sum_{n,m=1}^{\infty} \frac{2na^4 w_x^2 w_y^2}{\nu L_x^2 L_y Q_1}\alpha\Phi e^{-2\gamma_1}, \tag{A.3}$$

$$\frac{d}{dz}\left[a^2 w_x w_y V_y\right] = \sum_{n,m=1}^{\infty} \frac{2ma^4 w_x^2 w_y^2}{\nu L_x L_y^2 Q_1}\alpha\Phi e^{-2\gamma_1}, \tag{A.4}$$

$$\frac{d}{dz}\left[a^2 w_x^3 w_y\right] = 4a^2 w_x^3 w_y B, \tag{A.5}$$

$$\frac{d}{dz}\left[a^2 w_x w_y^3\right] = 4a^2 w_x w_y^3 C, \tag{A.6}$$

$$\frac{d\phi}{dz} = \frac{(w_x^2 + w_y^2)\Theta}{(w_x^2 - w_y^2)}, \tag{A.7}$$

$$\frac{d}{dz}\left[a^2 w_x w_y (w_x^2 - w_y^2)\Theta\right] = \sum_{n,m=1}^{\infty} \frac{2\pi a^4 w_x^2 w_y^2 \alpha e^{-2\gamma_1}}{\nu L_x L_y \rho_1 Q_1}\left[\chi - \frac{\alpha M \rho_3}{\rho_1}\right] \tag{A.8}$$

$$\begin{aligned}\sigma' + \frac{1}{4}\left[w_x^2 B' + w_y^2 C' - (w_x^2 - w_y^2)\Theta\phi'\right] &= \frac{1}{2}\left(V_x^2 + V_y^2\right) - \frac{1}{2}\left(w_x^2 B^2 + w_y^2 C^2\right) \\ - \frac{(w_x^2 + w_y^2)}{2w_x^2 w_y^2}\left(1 + \frac{w_x^2 w_y^2 \Theta^2}{4}\right) &+ \sum_{n,m=1}^{\infty} \frac{2a^2 w_x w_y \alpha^2 e^{-2\gamma_1}}{\pi\nu L_x L_y Q_1},\end{aligned} \tag{A.9}$$

$$\sigma' + \frac{1}{4}\left(3w_x^2 B' + w_y^2 C' - (3w_x^2 + w_y^2)\Theta\phi'\right) = \tag{A.10}$$

$$\begin{aligned}&\frac{1}{2}\left(V_x^2 + V_y^2\right) - \frac{1}{2}\left(3w_x^2 B^2 + w_y^2 C^2 - \frac{1}{w_x^2} + \frac{1}{w_y^2} + \frac{(3w_x^2 + w_y^2)\Theta^2}{4}\right) \\ &+ \sum_{n,m=1}^{\infty} \frac{a^2 w_x w_y \alpha e^{-2\gamma_1}}{2\pi\nu L_x L_y Q_1}\left[\alpha\left(4 - \frac{\pi^2 \cos^2\phi M}{w_x^2 \rho_1^2}\right) - \frac{\pi^2 w_y^2}{\rho_1}\left(w_x^2 G_2 - \frac{n\sin(2\phi)G}{L_x}\right)\right],\end{aligned} \tag{A.11}$$

$$\sigma' + \frac{1}{4}\left(w_x^2 B' + 3w_y^2 C' - (w_x^2 - 3w_y^2)\Theta\phi'\right) = \tag{A.12}$$

$$\begin{aligned}&\frac{1}{2}\left(V_x^2 + V_y^2\right) - \frac{1}{2}\left(w_x^2 B^2 + 3w_y^2 C^2 + \frac{1}{w_x^2} - \frac{1}{w_y^2} + \frac{(w_x^2 + 3w_y^2)\Theta^2}{4}\right) \\ &+ \sum_{n,m=1}^{\infty} \frac{a^2 w_x w_y \alpha e^{-2\gamma_1}}{2\pi\nu L_x L_y Q_1}\left[\alpha\left(4 - \frac{\pi^2 \sin^2\phi M}{w_y^2 \rho_1^2}\right) - \frac{\pi^2 w_x^2}{\rho_1}\left(w_y^2 G_2 + \frac{n\sin(2\phi)G}{L_x}\right)\right].\end{aligned} \tag{A.13}$$

for the elliptical beam evolution. Here

$$\Phi = e^{-U_+}\sin\vartheta_- - e^{-U_-}\sin\vartheta_+, \tag{A.14}$$

$$M = \frac{n^2}{L_x^2} + w_x^2 w_y^2 \psi_+ \psi_-, \tag{A.15}$$

$$\chi = \frac{n\cos(2\phi)(w_x^2 - w_y^2)G}{L_x}, \tag{A.16}$$

$$G = \psi_+ e^{-U_+}\cos\vartheta_- - \psi_- e^{-U_-}\cos\vartheta_+, \tag{A.17}$$

$$G_2 = \psi_+^2 e^{-U_+}\cos\vartheta_- - \psi_-^2 e^{-U_-}\cos\vartheta_+. \tag{A.18}$$

Appendix B. Variational Equations: Modulation Theory

The modulation equations for the shelf method, including the loss to shed radiation, are

$$\frac{d}{dz}\left[\frac{a^2 w_x w_y}{4} + g^2\Lambda\right] = -2\delta\Lambda\kappa^2, \tag{B.1}$$

$$a' w_x w_y + a w_x' w_y + a w_x w_y' - 2g\Lambda\sigma' = -g\Lambda\left(V_x^2 + V_y^2\right), \tag{B.2}$$

$$\xi' = V_x, \quad \eta' = V_y, \tag{B.3}$$

$$\frac{d}{dz}\left[\left(\frac{a^2 w_x w_y}{4} + g^2\Lambda\right)V_x\right] = -\sum_{n,m=1}^{\infty}\frac{n a^4 w_x^2 w_y^2 \alpha\Phi e^{-\gamma_1}}{2\nu L_x^2 L_y Q_1}, \tag{B.4}$$

$$\frac{d}{dz}\left[\left(\frac{a^2 w_x w_y}{4} + g^2\Lambda\right)V_y\right] = \sum_{n,m=1}^{\infty}\frac{m a^4 w_x^2 w_y^2 \alpha\Phi e^{-\gamma_1}}{2\nu L_x L_y^2 Q_1}, \tag{B.5}$$

$$\phi' = \frac{\left(w_x^2 + w_y^2\right)}{\left(w_x^2 - w_y^2\right)}\Theta, \tag{B.6}$$

$$\begin{aligned}&\frac{d}{dz}\left[\left(a^2 w_x w_y\left(w_x^2 - w_y^2\right)\right)\Theta\right]\\ &\quad= \sum_{n,m=1}^{\infty}\frac{2\pi a^4 w_x^2 w_y^2 \alpha e^{-\gamma_1}}{\nu L_x L_y Q_1 \rho_1}\left[\frac{n\cos(2\phi)\left(w_x^2 - w_y^2\right)G}{L_x} - \frac{\alpha M \rho_3}{\rho_1}\right],\end{aligned} \tag{B.7}$$

$$\begin{aligned}\frac{dg}{dz} &= \frac{a}{4w_x^2} + \frac{a}{4w_y^2} + \frac{a\left(w_x^2 w_y^2\right)\Theta^2}{16} - 2\delta g\\ &- \sum_{n,m=1}^{\infty}\frac{a^3 w_x w_y \alpha e^{-\gamma_1}}{8\pi\nu L_x L_y Q_1 \rho_1}\left[\pi^2\alpha M + 2\pi^2 w_x^2 w_y^2 G_2 + \frac{\pi^2 n\sin(2\phi)\left(w_x^2 - w_y^2\right)G}{L_x}\right],\end{aligned} \tag{B.8}$$

$$\begin{aligned}\frac{d\sigma}{dz} &= \frac{1}{2}\left(V_x^2 + V_y^2\right) - \frac{1}{w_x^2} - \frac{1}{w_y^2} + \sum_{n,m=1}^{\infty}\frac{a^2 w_x w_y \alpha e^{-\gamma}}{4\pi\nu L_x L_y Q_1}\\ &\times\left[\alpha\left(8 + \frac{\pi^2 M}{\rho_1}\right) + \frac{2\pi^2 w_x^2 w_y^2 G_2}{\rho_1} + \frac{\pi^2 n\sin(2\phi)\left(w_x^2 - w_y^2\right)G}{L_x}\right].\end{aligned} \tag{B.9}$$

The algebraic equation for Θ is given by

$$\Theta^2 = \frac{\left(w_x^2 - w_y^2\right)}{D}\left[-\sum_{n,m=1}^{\infty}\frac{2\pi a^2 w_x w_y \alpha e^{-\gamma_1}(W - F)}{\nu L_x L_y Q_1 \rho_1}\right] - \frac{4}{w_x^2} + \frac{4}{w_y^2}, \tag{B.10}$$

where

$$D = w_x^4 + 6w_x^2 w_y^2 + w_y^4, \tag{B.11}$$

$$F = \frac{\alpha M}{\rho_1}\left(\frac{\cos^2\phi}{w_x^2} - \frac{\sin^2\phi}{w_y^2}\right), \tag{B.12}$$

$$W = \frac{n\sin(2\phi)\left(w_x^2 + w_y^2\right)G}{L_x}. \tag{B.13}$$

The loss coefficient δ is

$$\delta = -\frac{\sqrt{2\pi}}{32e\kappa\tilde{\Lambda}}\int_0^z \pi\kappa(z')\ln[(z-z')/\tilde{\Lambda}]\frac{dz'}{(z-z')}\times$$
$$\left[\left(\left\{\frac{1}{2}\ln[(z-z')/\tilde{\Lambda}]\right\}^2 + \frac{3\pi^2}{4}\right)^2 + \pi^2\left\{\ln[(z-z')/\tilde{\Lambda}]\right\}^2\right]^{-1}, \tag{B.14}$$

where

$$\kappa^2 = \frac{1}{\tilde{\Lambda}}\left[\frac{1}{4}a^2 w_x w_y - \frac{1}{4}\hat{a}^2\hat{w}^2 + \tilde{\Lambda}g^2\right]. \tag{B.15}$$

The nonlocality of the NLC shifts the point at which the solitary wave sheds diffractive radiation from the edge of the shelf $\sqrt{w_y^2X^2 + w_x^2Y^2} = w_x w_y$ to a new radius $\tilde{\ell}$ from the solitary wave position (ξ, η), which is the edge of the director response [29]. This radius for the radiation response was termed the outer shelf radius [29]. In the present case of a finite cell, the director response extends to the cell walls. Hence,

$$\tilde{\Lambda} = \tilde{\ell}^2/2 \tag{B.16}$$

where

$$\tilde{\ell} = \min\left(\frac{L_x}{2}, \frac{L_y}{2}\right). \tag{B.17}$$

In the case of a finite cell, the diffractive radiation is then shed in a boundary layer at the cell walls.

[1] G. Assanto, M. Peccianti and C. Conti "Nematicons: Optical spatial solitons in nematic liquid crystals," *Optics & Photonics News*, **14**, 44–48 (2003).

[2] M. Peccianti and G. Assanto, "Nematicons," *Phys. Reports,* **516**, 147–208 (2012).

[3] Ed. by G. Assanto, "Nematicons; spatial optical solitons in nematic liquid crystals," *John Wiley and Sons*,**1**, (2013).

[4] M. Peccianti, A. De Rossi, G. Assanto, A. De Luca, C. Umeton and I.C. Khoo, "Electrically assisted self-confinement and waveguiding in planar nematic liquid crystal cells," *App. Phys. Lett.*, **91**, 7–9 (2000).

[5] E.A. Kuznetsov and A.M. Rubenchik, "Soliton stabilization in plasmas and hydrodynamics," *Phys. Reports.*, **142**, 103–165 (1986).

[6] Yu.S. Kivshar and G. Agrawal, *Optical Solitons: From Fibers to Photonic Crystals*, Academic Press, San Diego, (2003).

[7] A. Cheskidov, D.D. Holm, E. Olson and E.S. Titi, "On a Leray-α model of turbulence," *Proc. R. Soc. Lond. A*, **461**, 629–649 (2005).

[8] A. Ilyin, E.M. Lunasin and E.S. Titi, "A modified-Leray-α subgrid scale model of turbulence," *Nonlinearity*, **19**, 879–897 (2006).

[9] E.D. Eugenieva, D.N. Christodoulides and M. Segev, "Elliptic incoherent solitons in saturable nonlinear media," *Opt. Lett.*, **25**, 972–974 (2000).
[10] O. Katz, T. Cannon, T. Schwartz, M. Segev and D.N. Christodoulides, "Observation of elliptic incoherent spatial solitons," *Opt. Lett.*, **29**, 1248 – 1250 (2004).
[11] B. Crosignani and P. Di Porta, "Nonlinear propagation in Kerr media of beams with unequal transverse widths," *Opt. Lett.*, **18**, 1394–1396 (1993).
[12] O. Bang, W. Królikowski, J. Wyller and J.J. Rasmussen, "Collapse arrest and soliton stabilization in nonlocal nonlinear media," *Phys. Rev. E*, **66**, 046619 (2002).
[13] A.S. Desyatnikov, D. Buccoliero, M.R. Dennis and Yu.S. Kivshar, "Suppression of Collapse for Spiraling Elliptic Solitons," *Phys. Rev. Lett.*, **104**, 053902 (2010).
[14] R.Y. Chiao, E. Garmine and C.H. Townes, "Self-trapping of Optical Beams," *Phys. Rev. Lett.*, **13**, 479–482 (1964).
[15] A. Barthelemy, C. Froehly, S. Maneuf and E. Reynaud, "Experimental observation of beams' self-deflection appearing with two-dimensional spatial soliton propagation in bulk Kerr material," *Opt. Lett.*, **17**, 844–846 (1992).
[16] L. Marrucci, F. Vetrano and E. Santamato, "Optical reorientation in nematic liquid crystals controlled by the laser beam shape," *Opt. Comm.*, **171**, 131–136 (1999).
[17] I.C. Khoo, *Liquid Crystals: Physical Properties and Nonlinear Optical Phenomena,* Wiley, New York (1995).
[18] I.C. Khoo, "Nonlinear optics of liquid crystalline materials," *Phys. Rep.,* **471**, 221–267 (2009).
[19] I.C. Khoo, "Theory of optically induced molecular reorientations and quantitative experiments on wave mixing and the self-focusing of light," *Phys. Rev. A*, **25**, 1636–1644 (1982).
[20] M. Peccianti, K.A. Brzdakiewicz and G. Assanto, "Nonlocal spatial soliton interactions in nematic liquid crystals," *Opt. Lett.,* **27**, 1460–1462 (2002).
[21] A. Alberucci, G. Assanto, D. Buccoliero, A.S. Desyatnikov, T.R. Marchant and N.F. Smyth, "Modulation analysis of boundary-induced motion of optical solitary waves in a nematic liquid crystal," *Phys. Rev. A*, **79**, 043816 (2009).
[22] A.A. Minzoni, L.W. Sciberras, N.F. Smyth and A.L. Worthy, "Propagation of optical spatial solitary waves in bias-free nematic-liquid-crystal cells," *Phys. Rev. A*, **84**, 043823 (2011).
[23] A.A. Minzoni, L.W. Sciberras, N.F. Smyth and A.L. Worthy, "Optical vortex solitary wave in a bounded nematic-liquid-crystal cell," *Phys. Rev. A*, **87**, 013810 (2013).
[24] G.B. Whitham, *Linear and Nonlinear Waves*, J. Wiley and Sons, New York, (1974).
[25] D. Anderson, "Variational approach to nonlinear pulse propagation in optical fibers," *Phys. Rev. A*, **27**, 3135–963145 (1983).
[26] B. Malomed, "Variational methods in nonlinear fiber optics and related fields," *Prog. Opt.*, **43**, 71–193 (2002).
[27] B.D. Skuse and N.F. Smyth, "Interaction of two-color solitary waves in a liquid crystal in the nonlocal regime," *Phys. Rev. A*, **79**, 063806 (2009).
[28] A.A. Minzoni, N.F. Smyth, A.L. Worthy and Y.S. Kivshar, "Stabilization of vortex solitons in nonlocal nonlinear media," *Phys. Rev. A*, **76**, 063803 (2007).
[29] A.A. Minzoni, N.F. Smyth and A.L. Worthy, "Modulation solutions for nematicon propagation in nonlocal liquid crystals," *J. Opt. Soc. Amer. B*, **24**, 1549–1556 (2007).
[30] B.D. Skuse and N.F. Smyth, "Two-colour vector soliton interactions in nematic liquid crystals in the local response regime," *Phys. Rev. A*, **77**, 013817 (2008).
[31] A.A. Minzoni, N.F. Smyth and Z. Xu, "Stability of an optical vortex in a circular nematic cell," *Phys. Rev. A*, **81**, 033816 (2010).
[32] N.F. Smyth and W. Xia, "Refraction and instability of optical vortices at an interface in a liquid crystal," *J. Phys. B: At. Mol. Opt. Phys.*, **45**, 165403 (2012).
[33] G. Assanto, A.A. Minzoni, N.F. Smyth and A.L. Worthy, "Refraction of nonlinear beams by localised refractive index changes in nematic liquid crystals," *Phys. Rev. A*, **82**, 053843 (2010).
[34] G. Assanto, A.A. Minzoni, M. Peccianti and N.F. Smyth, "Optical solitary waves escaping a wide trapping potential in nematic liquid crystals: modulation theory," *Phys. Rev. A*, **79**, 033837 (2009).
[35] G. Assanto, N.F. Smyth and W. Xia, "Modulation analysis of nonlinear beam refraction at an interface in liquid crystals," *Phys. Rev. A*, **84**, 033818 (2011).
[36] G. Assanto, N.F. Smyth and W. Xia, "Refraction of nonlinear light beams in nematic liquid crystals," *J. Nonlin. Opt. Phys. Mater.*, **21**, 1250033 (2012).
[37] M. Peccianti and G. Assanto, "Nematic liquid crystal: A suitable medium for self-confinement of coherent and incoherent light," *Phys. Rev. E*, **65**, 035603(R) (2002).
[38] C. Conti, M. Peccianti and G. Assanto, "Route to nonlocality and observation of accessible solitons,"

Phys. Rev. Lett., **91**, 073901 (2003).
[39] A. Alberucci, M. Peccianti and G. Assanto, "Nonlinear bouncing of nonlocal spatial solitons at boundaries," *Opt. Lett.*, **32**, 2795–2797 (2007).
[40] A. Alberucci and G. Assanto, "Propagation of optical spatial solitons in finite-size media: interplay between nonlocality and boundary conditions," *J. Opt. Soc. Amer. B*, **24**, 2314–2320 (2007).
[41] W.L. Kath and N.F. Smyth, "Soliton evolution and radiation loss for the nonlinear Schrodinger equation," *Phys. Rev. E*, **51**, 1484–1492 (1995).
[42] A. Alberucci, A. Piccardi, M. Peccianti, M. Kaczmarek and G. Assanto, "Propagation of spatial optical solitons in a dielectric with adjustable nonlinearity," *Phys. Rev. A*, **82**, 023806 (2010).
[43] A.W. Snyder, and M.J. Mitchell, "Accessible solitons," *Science*, **276**, 1538–1541 (1997).
[44] J. Yang, "Vector solitons and their internal oscillations in birefringent nonlinear optical fibers," *Stud. Appl. Math.*, **98**, 61–97 (1997).
[45] D.J. Kaup and A.C. Newell, "Solitons as particles, oscillators, and in slowly changing media: a singular perturbation theory," *Proc. Roy. Soc. Lond. A*, **361**, 413–446 (1978).
[46] A.A. Minzoni, N.F. Smyth and A.L. Worthy, "Pulse evolution for a two dimensional Sine-Gordon equation," *Physica D*, **159**, 101–123 (2001).
[47] G. Assanto, B.D. Skuse and N.F. Smyth, "Optical path control of spatial optical solitary waves in dye-doped nematic liquid crystals," *Photon. Lett. Poland*, **1**, 154–156 (2009).
[48] G. Assanto, B.D. Skuse and N.F. Smyth, "Solitary wave propagation and steering through light-induced refractive potentials," *Phys. Rev. A*, **81**, 063811 (2010).
[49] G. Liang and Q. Guo, "Spiraling elliptic solitons in nonlocal nonlinear media without anisotropy," *Phys. Rev. A*, **88**, 043825 (2013).